Energy Efficient Visible Light Communications Relying on Amorphous Cells

Rong Zhang [1], Holger Claussen[2], Harald Haas[3], and Lajos Hanzo[1]

[1]Southampton Wireless, School of ECS, University of Southampton, SO17 1BJ, UK
[2]Small Cells Research, Bell Laboratories, Alcatel-Lucent, Dublin 15, Ireland
[3]Li-Fi R&D Centre, Institute for Digital Communications, University of Edinburgh, EH9 3JL, UK

***Abstract*—In this paper, we design an energy efficient indoor Visible Light Communications (VLC) system from a radically new perspective based on an amorphous user-to-network association structure. Explicitly, this intriguing problem is approached from three inter-linked perspectives, considering the cell formation, link-level transmission and system-level optimisation, critically appraising the related optical constraints. To elaborate, apart from proposing hitherto unexplored Amorphous Cells (A-Cells), we employ a powerful amalgam of Asymmetrically Clipped Optical Orthogonal Frequency Division Multiplexing (ACO-OFDM) and transmitter pre-coding aided Multi-Input Single-Output (MISO) transmission. As far as the overall system-level optimisation is concerned, we propose a low-complexity solution dispensing with the classic Dinkelbach's algorithmic structure. Our numerical study compares a range of different cell formation strategies and investigates diverse design aspects of the proposed A-Cells. Specifically, our results show that the A-Cells proposed are capable of achieving a much higher energy efficiency per user compared to that of the conventional cell formation for a range of practical Field of Views (FoVs) angles.**

***Index Terms*—Energy Efficiency, Optical Wireless, Small Cells, Optical OFDM, Optical MIMO**

I. Introduction

1) Background: Improving the attainable energy efficiency has been one of the salient design objectives of modern wireless communications [1]. In the post-4G era, quantifying energy efficiency became a challenge owing to the emerging Heterogeneous Networks (HetNet) in pursuit of 'green' designs [2]–[6]. With the launch of the global 5G research initiatives, the community expanded its horizon from Radio Frequency (RF) cellular networks both to millimetre wave [7] and to optical wireless concepts [8]. Owing to this paradigm-shift to higher frequencies, the disruptive large-scale Multi-Input Multi-Output (MIMO) architecture has attracted substantial interests, with the goal of further improving the achievable energy efficiency [9]. Apart from the classic perspectives on energy efficiency, the novel concepts of wirelessly powered communications [10], [11] are also emerging. Despite all the above advances, there is a paucity of literature on designing energy efficient optical wireless systems, especially indoor Visible Light Communications (VLC) systems.

With the advent of high-power Light Emitting Diodes (LEDs) and high-sensitivity Photo-Diodes (PD), the VLC concept appears to be especially promising in the small-cell family of the 5G era [12]. By modulating the visible light produced by the LEDs way above the human eye's fusion frequency, the dual goal of communication and illumination can be realised simultaneously. The pioneering implementation of VLC using LEDs was carried out by the Nakagawa laboratory in 2004 [13], which stimulated significant research attention. The link-level data rates of 100s of MBits/s have been reported using state-of-the-art LEDs and photo-detectors [14]. The modulation schemes have evolved from simple pulse based modulation to more sophisticated Asymmetrically Clipped / DC-biased Optical Orthogonal Frequency Division Multiplexing (ACO/DCO-OFDM) [15], [16]. More ambitious GBits/s targets have also been achieved with the aid of optical MIMO techniques [17] and by using advanced LEDs [18]. Apart from these exciting link-level achievements, the system-level study of VLC has also been developed for broadening its scope beyond point-to-point applications [19]–[24].

2) Motivation: However, most of the above-mentioned VLC research aimed for increasing the attainable throughput, whilst paying less attention to energy efficiency. In fact, LEDs are primarily used for illumination, where typically a constant DC power is provided to satisfy the illumination requirements and to maintain sufficient forward biasing voltages across the LEDs for communications. Hence, the additional communication function should not perturb the illumination requirements nor should it violate the LEDs physical limits. Desirably, the extra communication-related power consumption invested should also be as low as possible, while maintaining a minimum required Quality of Service (QoS). This is also true when no illumination is required during daytime. Hence, valuable research has been dedicated to link-level energy efficiency focusing on brightness and dimming control with the aid of both modulation-related [25], [26] and coding-related [27], [28] techniques. However, there is no system-level investigation on energy efficient VLC systems supporting multi-users, which may require a radically new design approach.

When considering the attainable system-level energy efficiency of a particular network, the specific structure of associating the users with the network plays a crucial role. As a re-

Manuscript received: Apr 2015. Manuscript revised: Sep 2015. The financial support of the EPSRC project (EP/N004558/1) and that of the EU under the Concerto project as well as that of the European Research Council's (ERC) Advanced Fellow Grant is gratefully acknowledged. The data from the paper can be obtained from the University of Southampton ePrints research repository: 10.5258/SOTON/385179.

sult, it has limited benefits to optimise the power consumption of an inefficient user-to-network association structure. Thanks to the flexibility in indoor VLC systems design [12], we advocate an *amorphous* user-to-network association structure for indoor VLC systems. To elaborate, in conventional structures, the cells are typically formed from a network-centric perspective, without taking into account the users' positions, where the design flow is based on defining a cell constituted by one or more Access Points (APs) and then associating the users with it. In RF cellular systems having hundreds or thousands of random uniformly distributed users, the conventional structure may indeed be applicable. However, when considering an indoor VLC system supporting only a few dozen users, naively applying the conventional structure may become inefficient, since the users are sporadic. Moreover, in VLC systems, the number of APs may be higher than the number of users, creating an ultra dense AP deployment. Hence, we propose Amorphous Cells (A-Cells) from a user-centric point of view by considering the users' positions, where the design flow is based on grouping the users together and then associating the APs with them, resulting in irregular shape cells.

3) Scope: We design an energy efficient indoor VLC system relying on an amorphous structure under practical optical constraints by considering three interlinked design aspects, namely the cell formation, the link-level transmission and the system-level power allocation. Logically, the cell formation strategy determines the specific association between the APs and users, while the transmission strategy and the power allocation jointly determine the signal strength and the amount of interference. Explicitly,

- we propose two A-Cells formation techniques, namely the *edge-distance* and *centroid-distance* based A-Cells. The beneficial construction of A-Cells constitutes the basis of a structurally energy efficient indoor VLC system;
- we propose a new link-level transmission scheme by amalgamating the ACO-OFDM and our Vector Transmission (VT) and Combined Transmission (CT) based Multiple Input Single Output (MISO) transmission of [12];
- we propose an efficient low-complexity algorithm for maximising the system-level energy efficiency employing the advocated link-level transmission scheme associated with the proposed A-Cells.

Our paper is organised as follows. In Section II-A, we embark on designing the proposed amorphous structure, while in Section II-B, we discuss the transmission schemes employed and finally we perform system optimisation in Section II-C. The achievable performance of our design is characterised in Section III and we close in Section IV.

II. System Description

Consider an indoor VLC environment having N APs uniformly installed on the ceiling, where each AP is constituted by an array of L LEDs pointing vertically downwards. These APs will be used for communicating with K users and at the same time for providing illumination. As discussed before, supporting wireless communications should not violate the main illumination requirements and should obey the LEDs physical limits. Hence, the communications-related power investment should be as low as possible in order to minimise the perturbations imposed on the lightening function, while maintaining a minimum required QoS. This leads to communications-related energy efficiency maximisation as

$$\max_{\mathcal{F},\mathcal{T},\mathcal{P}} f_t(\mathcal{F},\mathcal{T},\mathcal{P})/f_p(\mathcal{F},\mathcal{T},\mathcal{P}), \quad (1)$$

where $f_t(\cdot)$ represents the achievable throughput, which is a function of the cell formation strategy $\mathcal{F}$, of the link-level transmission strategy $\mathcal{T}$ and of the power allocation strategy $\mathcal{P}$. Furthermore, $f_p(\cdot)$ represents the power consumption, which is also a function of $\mathcal{F}$, $\mathcal{T}$ and $\mathcal{P}$. Since $\mathcal{F}$ and $\mathcal{T}$ are potentially enumerable, we can reformulate (1) given $\mathcal{F}$ and $\mathcal{T}$ as [1].

$$\max_{\mathcal{P}} f_{t|\mathcal{F},\mathcal{T}}(\mathcal{P})/f_{p|\mathcal{F},\mathcal{T}}(\mathcal{P}). \quad (2)$$

To adopt a clear structure, we will elaborate 1) on the cell formation strategy in Section II-A by describing the channel characteristics in Section II-A1, then introducing the motivation of A-Cells in Section II-A2 and finally detailing the construction of A-Cells in Section II-A3; 2) on the transmission strategy in Section II-B by introducing ACO-OFDM and MISO transmission in Section II-B1 and Section II-B2 respectively, and then introducing the optical constraints in Section II-B3; 3) on the power allocation strategy in Section II-C by outlining our problem formulation, transformation and simplification in Section II-C1, Section II-C2 and Section II-C3, respectively.

A. Amorphous Structure

Fixing $\mathcal{F}$ in (1) not only reduces the complexity of the problem, but also constitutes a logically appealing arrangement, since cell formation is the pivotal system design stage.

1) Channel Characteristics: Before introducing the cell formation strategy, a brief description of the VLC channel characteristics is essential. The optical channel between the kth user and the nth AP is constituted by both the direct Line-of-Sight (LoS) component $h^0_{k,n}$ and its reflections, but we only consider the first reflection $h^1_{k,n}$, since higher-order indirect reflections are typically negligible. Specifically, the LoS component is given by [13]

$$h^0_{k,n} = \frac{(m_L+1)A_{PD}}{2\pi d^2}\cos^{m_L}(\theta)\cos(\psi)f_{of}(\psi)f_{oc}(\psi), \quad (3)$$

where the Lambert index $m_L = -1/\log_2\left[\cos(\phi_{1/2})\right]$ depends on the semi-angle $\phi_{1/2}$ at half-illumination of the source. A_{PD} is the physical area of the PD receiver, d is the distance between the kth user and the nth AP, θ is the angle of irradiance from the nth AP and ψ is the angle of incidence at the kth user. Still referring to (3), $f_{of}(\psi)$ and $f_{oc}(\psi)$ denote the gain of the optical filter and of the optical concentrator employed, respectively. Furthermore, $f_{oc}(\psi)$ can be written as

$$f_{oc}(\psi) = n_r^2/\sin^2(\psi), \psi \le \psi_F; \quad f_{oc}(\psi) = 0, \psi > \psi_F, \quad (4)$$

[1]Re-evaluating (2) upon the change of cell formation and transmission strategy would impose an excessive complexity. Fortunately, indoor VLC systems typically have low-mobility. Hence, updating (2) semi-adaptively, not instantaneously, strikes a comprise, although the optimal updating frequency is application-specific. However, these interesting points are out of our scope.

where ψ_F represents half of the receiver's Field-of-View (FoV) and n_r is the refractive index of a lens at a PD receiver. By contrast, the first reflected component is given by [13]

$$h^1_{k,n} = \sum_{v}\sum_{\tau} \frac{\rho_r A_r d^2}{d^2_{v,\tau,1} d^2_{v,\tau,2}} \cos(\alpha_{v,\tau}) \cos(\beta_{v,\tau}) h^0_{k,n}, \quad (5)$$

where $d_{v,\tau,1}$ is the distance between the nth AP and the (v,τ)th reflection point, while $d_{v,\tau,2}$ is the distance between the (v,τ)th reflection point and the kth user. Furthermore, $\alpha_{v,\tau}$ and $\beta_{v,\tau}$ denote the angle of incidence for the incoming light and the angle of irradiance for the outgoing light at the (v,τ)th reflection point, having a tiny area of A_r and a reflectance factor of ρ_r. Furthermore, the pair of summations in (5) represent all the reflections from the walls. Finally, the aggregated channel between the kth user and the nth AP is given by $h_{k,n} = h^0_{k,n} + h^1_{k,n}$, where we assumed single-tap channel response. In the following, we use only the LoS component for constructing the A-Cells, but we will use the aggregated channel for the rest of our design.

2) Motivation of A-Cells: Fig 1 portrays the conventional structure (left) and the amorphous structure (right) for a 15m×15m indoor VLC system having 8×8 APs (marked by squares) and 20 users (marked by circles) under three typical scenarios (same, more and less number of cells), where the users' positions are drawn from a uniform random distribution, whilst employing the parameters of Table I. Owing to space-limitations, in Fig 1 we only show the edge-distance based A-Cells having a predefined distance threshold of $d_0 = 3.5$m.

Conventional cells typically have a fixed shape. For example, we may partition the 15m×15m indoor environment into four square-shaped cells having $(4 \times 4) = 16$ APs per cell, where the users are associated with cells depending on the users' positions relative to the square-shaped boundary amongst the cells. Within each cell, we may switch off the communications function of the specific APs having no LoS links to the users in their vicinity (indicated by hollow small squares), since improving the energy efficiency is our goal. The related examples may be seen in the left of Fig 1, where we refer to this bench-marker as 'S16'. Similarly, we also have the special bench-marker of 'S1', which represents the scenario of using each AP to create an individual cell and again, the idle mode is used for those APs, which have no LoS links to the users in order to save energy [29].

A common observation concerning the conventional arrangement 'S16' in the left of Fig 1 is that the resultant cells are all constrained within the four partitioned areas. However, this arrangement may not be the most appropriate. For example, in the southwest cell of Fig 1a, the 'boundary user' 'A' is clearly far from user 'C' in the same cell, but it is more close to user 'B' in the neighbouring cell. Hence, there might be a tendency for user 'A' to separate from user 'C' and to join user 'B', as seen in Fig 1b of A-Cells. This is also true for the 'boundary user' 'D' in the northeast cell of Fig 1a, since it is more close to the users located in the southeast cell, than to the rest of the distant users in the same cell. More examples are shown in Fig 1c, where two clusters of boundary users highlighted by ellipses join A-Cells of Fig 1d. In addition to a different user-to-network association, the status

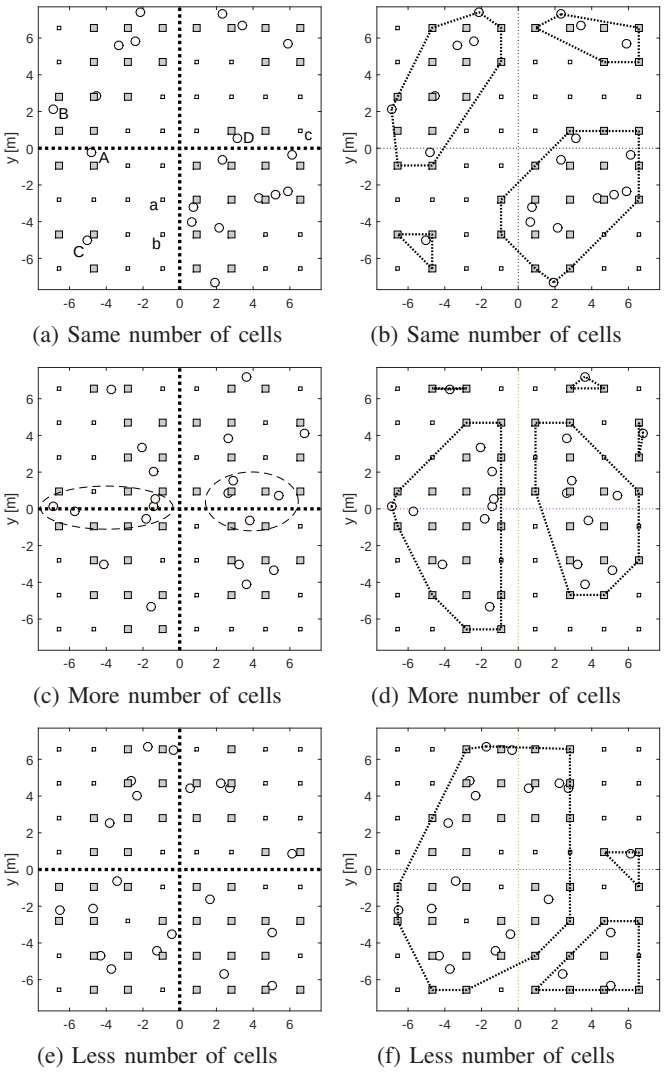

(a) Same number of cells (b) Same number of cells

(c) More number of cells (d) More number of cells

(e) Less number of cells (f) Less number of cells

Fig. 1: Illustration of the conventional (left) and the amorphous structure (right) for VLC indoor systems.

of APs is also different, where for example, APs ('a','b','c') were switched from idle mode in conventional cells of Fig 1a to become active in the A-Cell of Fig 1b, since they have LoS connections to the associated users. Hence, the proposed A-Cells are capable of *breaking boundaries*, leading to a higher and a lower number of A-Cells in Fig 1d and Fig 1f.

3) Construction of A-Cells: Let us first introduce some common notations. We let $\mathcal{C}$ be the specific set hosting all cells, where for the cth cell $\mathcal{C}_c$, we have $|\mathcal{N}_c|$ APs hosted in the set $\mathcal{N}_c$ serving $|\mathcal{K}_c|$ users of the set $\mathcal{K}_c$, with $|\cdot|$ being the cardinality of a set. Note that these notations are in generic sense, including both conventional cells and A-Cells. We are now ready to discuss the construction of A-Cells.

We firstly construct a *full* user-to-network association matrix $\boldsymbol{M}^f$ having K rows and N columns corresponding to K users and N APs [2]. The $[k,n]$th entry of $\boldsymbol{M}^f$ is set to the LoS

[2]The availability of the full user-to-network association matrix rely on the acquisition of channel knowledge at the AP side, which can be readily estimated at the user side and then fed back to the AP at the cost of a modest overhead. This is because the VLC channels are pre-dominantly static and the channel knowledge can be characterised by a single attenuation factor.

channel $h^0_{k,n}$. We then carry out *AP anchoring* as follows:

1) Initialise user-to-network association matrix $\boldsymbol{M} = \boldsymbol{M}^f$.
2) Find the best user-AP pair $[k^*, n^*]$ having the strongest LoS channel amongst all entries of $\boldsymbol{M}$ and then collect the best user-index k^* in $\boldsymbol{k}^*$.
3) Set all entries in the k^*th row and in the n^*th column of $\boldsymbol{M}$ to zero in order to exclude them from further consideration throughout the AP anchoring process.
4) If there are still positive entries in $\boldsymbol{M}$, we repeat this process from Step 2. Otherwise, we output $\boldsymbol{M}$ as the sub-matrix of $\boldsymbol{M}^f$ constituted by all rows from $\boldsymbol{k}^*$.

The objective of AP anchoring is to have exclusive user-AP pairs ensuring that each of those users in $\boldsymbol{k}^*$ will be served at least by its own anchor AP. Those users who have not found their anchor APs will be scheduled during the next anchoring round, however scheduling is beyond our current scope.

Having the user-to-network association matrix $\boldsymbol{M}$, the *distance based A-Cells* are constructed, where the users are firstly grouped based on a pre-defined distance threshold d_0 and then we select APs associated with those users [3] as follows:

1) Introduce the counter c, which is initialised as $c = 1$.
2) We commence forming cell $\mathcal{C}_c$ by recruiting the first user, who has not been included in any cells. Hence, this user will be the only one in the set $\mathcal{K}_c$ and along with the associated AP set $\mathcal{N}_c$ containing all the APs providing LoS connections to the first user.
3) Recruit another user from the set of hitherto unassigned users, who has the smallest distance from the edge/centroid of the cell $\mathcal{C}_c$, provided that their distance is shorter than d_0. In this step, the edge of the cell is characterised by connecting its containing users' positions. We then update cell $\mathcal{C}_c$, which results in the expanded set of $\mathcal{K}_c$ and $\mathcal{N}_c$.
4) We repeat Step 3 until no additional users can be grouped. As a result, we completed the update of cell $\mathcal{C}_c$, which resulted in the final set of $\mathcal{K}_c$ and $\mathcal{N}_c$.
5) Set all entries of the association matrix $\boldsymbol{M}$ associated with the users in $\mathcal{K}_c$ to zero. If there are still positive entries in $\boldsymbol{M}$, we increment c and repeat from Step 2.

Upon the completion of user grouping, we have to resolve the associated AP ambiguity, since some cells may have conflicting AP assignments. In those cases, any ambiguously assigned AP n is exclusively included in the c^*th cell containing those users to whom the ambiguously assigned AP n has the strongest LoS connection. Finally, note that the entire set of APs $\mathcal{N}_a$ involved in the ultimately constructed cells, namely $\mathcal{N}_a = \mathcal{N}_1 \cup \mathcal{N}_2 \cdots \cup \mathcal{N}_{|\mathcal{C}|}$, constitutes a subset of whole set of available APs in the room. For those unassigned APs in $\bar{\mathcal{N}}_a$, no communications are activated. To ease understanding, we include the pseudo-code in Algorithm 1. Regarding the complexity imposed, the first step of AP anchoring requires only an order of $\mathcal{O}(K)$ operations and an order of $\mathcal{O}(KN\log(KN))$ for finding the best user-AP pair. Furthermore, the complexity of Algorithm 1 is linear within the range of $[\mathcal{O}(K^2), \mathcal{O}(K^3)]$ owing to its hierarchical algorithmic structure.

[3]When constructing distance based A-Cells, the mutual distances between users are required. After acquiring the channel knowledge, the distances between users and APs can be inferred from (3). As a result, classical positioning may be used for determining the users' positions. Hence, the mutual distances between users can be readily calculated.

Algorithm 1 Distance based A-Cells

initialise $c = 1$, $\mathcal{K}_0 = \varnothing$
while $\boldsymbol{M} \succ \boldsymbol{0}$ **do**
  $k = \{\min k : k \notin \mathcal{K}_0\}$, $\boldsymbol{a} = \{\forall n : M[k,n] > 0\}$
  $\mathcal{C}_c : \{\mathcal{K}_c = \{k\}, \mathcal{N}_c = \{\boldsymbol{a}\}\}, \mathcal{K}^o_c = \varnothing$
  while $\mathcal{K}_c \neq \mathcal{K}^o_c$ **do**
    $\mathcal{K}^o_c = \mathcal{K}_c$, $\mathcal{K}_0 = \mathcal{K}_0 \cup \mathcal{K}_c$
    $k^* = \arg\min_{k \notin \mathcal{K}_0} \mathcal{D}(k, \mathcal{C}_c)$
    if $\mathcal{D}(k^*, \mathcal{C}_c) \leq d_0$ **then**
      $\boldsymbol{b} = \{\forall n : M[k^*, n] > 0\}$
      $\mathcal{C}_c : \{\mathcal{K}_c = \mathcal{K}_c \cup k^*, \mathcal{N}_c = \mathcal{N}_c \cup \boldsymbol{b}\}$
    end if
  end while
  $\boldsymbol{M}[\mathcal{K}_c, :] = \boldsymbol{0}$, $c = c + 1$
end while
for all $n \in \mathcal{N}_1 \cup \mathcal{N}_2 \cdots \cup \mathcal{N}_{|\mathcal{C}|}$ **do**
  $c^* = \arg\max_{\forall c}\{\max_{k \in \mathcal{K}_c} h^0_{k,n}\}$
  $\mathcal{N}_c = \mathcal{N}_c \setminus n, \quad \forall c \neq c^*$
end for

B. Link-level Transmission

Let us now discuss the transmission strategy relying on the amalgamation of ACO-OFDM and MISO transmission. Our forthcoming elaborations are equally applicable both to the conventional cells and to the proposed A-Cells.

1) ACO-OFDM: We first consider the downlink ACO-OFDM transmission from the nth AP $n \in \mathcal{N}_c$ to the kth user $k \in \mathcal{K}_c$ in the cth cell $\mathcal{C}_c$. Let N_s represent the number of ACO-OFDM sub-channels and let $\boldsymbol{s}_n \in \mathbb{C}^{N_s/4}$ represent the Frequency Domain (FD) information-bearing symbol vector transmitted from the nth AP. Then the resultant ACO-OFDM symbol vector $\boldsymbol{s}^f_n \in \mathbb{C}^{N_s}$ is constituted by the odd sub-channel entries of zero and the even sub-channel entries of

$$s^f_n[m] = \begin{cases} s_n[m/2] & \text{if } m \leq N_s/2 \text{ and is even} \\ s^{\text{conj}}_n[\frac{N_s - m + 2}{2}] & \text{if } m > N_s/2 \text{ and is even.} \end{cases} \quad (6)$$

It becomes plausible that the ACO-OFDM mapping of (6) obeys the Hermitian symmetry property, which allows us to create real-valued Time Domain (TD) signal samples $\boldsymbol{s}^t_n \in \mathbb{R}^{N_s}$ after the classic IFFT operation. Since the odd-indexed FD sub-channels are set to zero in the specific ACO-OFDM mapping of (6), the first-half of the TD signal samples are copied to the second-half of the TD signal samples, albeit with their signs flipped. As a result, the TD signal samples can be conveyed with all the negative parts clipped at zero. The clipping-distortion imposed by the removal of the negative amplitudes only occurs at the odd-indexed FD sub-channels carrying no data and hence can be ignored, despite the fact that the amplitude of the TD signal samples is halved.

The clipped positive and real-valued TD signal samples $\tilde{\boldsymbol{s}}^t_n \in \mathbb{R}^{N_s}_+$ in conjunction with the DC-bias current are then forwarded to the LEDs, where the TD signal envelope is

used for modulating the intensity of the LEDs. To elaborate a little further, the clipped TD signal samples $\tilde{\boldsymbol{s}}_n^t$ obey the clipped Gaussian distribution with a parameter of $\sigma_{s_n^t}$. Hence, the average optical power of the TD signal samples $\tilde{\boldsymbol{s}}_n^t$ is $P^o = \sigma_{s_n^t}/\sqrt{2\pi}$ and the total radiated optical power plus DC is $P = P^{dc} + P^o$. Correspondingly, the average electronic power of the TD signal samples $\boldsymbol{s}_n^t$ is $P_t^e = \sigma_{s_n^t}^2$, while the average electronic power of the FD ACO-OFDM symbol vector associated with its even-order half is $P_f^e = 2P_t^e$.

The kth user's receiver is comprised of a PD and a trans-impedance amplifier. After the removal of DC component and followed by direct detection relying on the Optical to Electrical (O/E) conversion factor of γ, the discrete-time model of the received FD symbol vector $\boldsymbol{y}_k \in \mathbb{C}^{N_s}$ after FFT becomes

$$\boldsymbol{y}_k = (\gamma/2)\text{diag}[\boldsymbol{h}]\boldsymbol{s}_n^f + \boldsymbol{I}_k + \boldsymbol{w}_k, \tag{7}$$

where $\boldsymbol{h} \in \mathbb{R}^{N_s}$ hosts the FD channel responses. Since the ACO-OFDM VLC channels can be safely considered as being non-dispersive for a bandwidth B upto 20 MHz [30], each entry of $\boldsymbol{h}$ becomes a single-tap gain factor $h_{k,n}$ [4]. Furthermore, $\boldsymbol{I}_k \in \mathbb{C}^{N_s}$ denotes the interference imposed on the kth user. Finally, $\boldsymbol{w}_k \in \mathbb{C}^{N_s}$ represents the noise vector accounting for both the shot noise and the thermal noise at the receiver, which can be modelled as zero-mean complex-valued AWGN with a variance of $\sigma^2 = N_0 B$, where $N_0 \approx 10^{-22}$ A^2/Hz [14]. Extracting the information-bearing sub-channels from $\boldsymbol{y}_k$, for each $m \in \{2, 4, \ldots, N_s/2\}$ we have,

$$y_k[m] = (\gamma/2)h_{k,n}s_n^f[m] + I_k[m] + w_k[m]. \tag{8}$$

Remark II-B1: Energy efficiency maximisation of conventional RF systems typically relies on Shannon's capacity expression for $f_t(\cdot)$ in (2), assuming Gaussian-distributed signalling. However, optical systems relying on Intensity Modulation/Direct Detection (IM/DD) can only have real-valued positive signals. Unfortunately, there is a lack of *exact* capacity expressions for optical systems, despite the existence of various forms of capacity bounds [31]. Hence, we consider ACO-OFDM, since it is a widely used optical modulation scheme exhibiting a higher power efficiency than DCO-OFDM, which allows us to derive an analytically tractable capacity expression [32], [33] for our energy efficiency maximisation problem to be discussed in Section II-C. Suffice to say that, the capacity expression of DCO-OFDM has to take into consideration the non-linear clipping distortion effects [33], which are hence set aside for our future research.

2) MISO Transmission: Having discussed the above point-to-point scenario, let us now discuss the multi-user scenario. For the cth cell having $|\mathcal{N}_c|$ APs and $|\mathcal{K}_c|$ users, the equivalent physical layer may be modelled as a multi-user MISO system for $|\mathcal{K}_c| > 1$ or as a single-user MISO system for $|\mathcal{K}_c| = 1$. In the former case, we employ VT based on Zero Forcing (ZF) Transmit Pre-Coding (TPC) for eliminating the inter-user-interference within the cth cell, while for the latter case, we employ CT for maximising the received signal power.

[4]We consider white LEDs constructed by using blue LEDs having a phosphor layer, which have a typical bandwidth of 20 MHz. This is achievable if a blue filter is used at the receiver side. Our methodology is also eminently applicable, when LEDs with $\geq$100 MHz bandwidth become available.

When $|\mathcal{K}_c| = 1$, CT is employed, where we transmit the same signal $s_n^f[m] = x_{k_0}[m]$ from all $n \in \mathcal{N}_c$ APs to the only user $k_0 \in \mathcal{K}_c$. The signals arriving at the k_0th receiver can be constructively combined, since all the channels emerging from all $\mathcal{N}_c$ APs to the user k_0 are positive. Hence, for the mth sub-channel $m \in \{2, 4, \ldots, N_s/2\}$, we have the single-user MISO expression of (8) written as

$$y_{k_0}[m] = (\gamma/2)\sum_{n\in\mathcal{N}_c} h_{k_0,n}\varrho_n^{ct}x_{k_0}[m] + I_{k_0}[m] + w_{k_0}[m], \tag{9}$$

where we set normalised electronic power of $x_{k_0}[m]$ being unity and let $\varrho_n^{ct} = \sqrt{2P_{c,n}^{ct}}$ with $P_{c,n}^{ct}$ to be optimised. By contrast, for $|\mathcal{K}_c| > 1$, VT is employed. For the mth sub-channel $m \in \{2, 4, \ldots, N_s/2\}$, we have the multi-user MISO expression of (8) written as

$$\boldsymbol{y}[m] = (\gamma/2)\boldsymbol{H}\boldsymbol{s}^f[m] + \boldsymbol{I}[m] + \boldsymbol{w}[m], \tag{10}$$

where $\boldsymbol{y}[m] \in \mathbb{C}^{|\mathcal{K}_c|}$ is the received FD symbol vector of all the $|\mathcal{K}_c|$ users in the cth cell on the mth sub-channel, while $\boldsymbol{s}^f[m] \in \mathbb{C}^{|\mathcal{N}_c|}$ is the FD symbol vector transmitted from all $|\mathcal{N}_c|$ APs in the cth cell on the mth sub-channel. Finally, $\boldsymbol{H} \in \mathbb{R}^{|\mathcal{K}_c|\times|\mathcal{N}_c|}$ is the channel between the $|\mathcal{K}_c|$ users and the $|\mathcal{N}_c|$ APs, while $\boldsymbol{I}[m] \in \mathbb{C}^{|\mathcal{K}_c|}$ is the inter-cell-interference imposed on all $|\mathcal{K}_c|$ users in the cth cell on the mth sub-channel. To eliminate the inter-user-interference, we employ TPC, which is formulated as $\boldsymbol{s}^f[m] = \boldsymbol{G}\boldsymbol{x}[m]$, where $\boldsymbol{x}[m] \in \mathbb{C}^{|\mathcal{K}_c|}$ is the multi-user FD symbol vector and the ZF precoding $\boldsymbol{G} \in \mathbb{R}^{|\mathcal{N}_c|\times|\mathcal{K}_c|}$ is explicitly formulated as $\boldsymbol{G} = \boldsymbol{H}^\dagger$, which is the pseudo-inverse of $\boldsymbol{H}$. Hence, (10) can be decomposed into $|\mathcal{K}_c|$ parallel streams and for any $k \in \mathcal{K}_c$, yielding

$$y_k[m] = (\gamma/2)\varrho_k^{vt}x_k[m] + I_k[m] + w_k[m], \tag{11}$$

where we set normalised electronic power of $x_k[m]$ being unity and let $\varrho_k^{vt} = \sqrt{2P_{c,k}^{vt}}$ with $P_{c,k}^{vt}$ to be optimised.

Remark II-B2: It is natural to consider multi-user MISO transmission in VLC systems using VT to eliminate the inter-user-interference. The roots of VT are in the celebrated results of information theory, where Dirty Paper Coding (DPC) is found to be capable of achieving the broadcast channel's capacity [34]. Owing to its non-linear complex nature of implementing DPC, the low-complexity ZF constitutes a popular alternative, which was shown to exhibit a negligible performance loss compared to DPC in the high Signal to Noise Ratio (SNR) regime, when the number of APs is larger than the number of users [35]. Hence, this important theoretical finding benefits directly a range of modern communications systems. For example, the concept of VT is similar to the successful employment of 'vectoring' in the state-of-the-art Digital Subscriber Line (DSL) based G.fast system invoked for coping with the crosstalk between twisted pairs. This operation is also reminiscent of the concept of the Coordinated Multiple Point (CoMP) transmission regime of classic RF cellular communications conceived for mitigating the inter-cell-interference at the cell edge [36]. In practice, to facilitate VT from $|\mathcal{N}_c|$ APs to $|\mathcal{K}_c|$ users, both the channel matrix $\boldsymbol{H}$ and the users' data $\boldsymbol{x}[m]$ have to be shared amongst the $|\mathcal{N}_c|$ APs. Fortunately, this requirement can be satisfied, since the

VLC channels are pre-predominately static, while the sharing of all users' data $\boldsymbol{x}[m]$ requires a more capable back-haul.

3) Optical Constraints: Typically, the forward current of the DC-biased and clipped TD signal samples should be within the LED's dynamic range [30]. Since the total radiated optical power is directly proportional to the forward current, we describe the optical constraints in terms of their optical power.

The total optical power radiated from an AP should satisfy the per-LED dynamic range of $P_{min} \leq P/L \leq P_{max}$, where we assume that each of the L LEDs constituting an AP emits the same optical power. For example, a practical dynamic range of a Vishay TSHG8200 LED is between $P_{min} = 5$ mW and $P_{max} = 50$ mW at room temperature. For satisfying a predefined illumination requirement constituted by the minimum illumination $\mathcal{I}_{min}$, the maximum illumination $\mathcal{I}_{max}$ and the average illumination $\mathcal{I}_{avg}$, we find the minimum required optical power P_{min}^{illu} by solving the problem of

$$P_{min}^{illu} = \min P \quad \text{s.t.} \tag{12}$$

$$\min_{\mu\in[1,K_p]} \sum_{n=1}^{N} h_{\mu,n}^{illu} P \geq \mathcal{I}_{min}, \quad \max_{\mu\in[1,K_p]} \sum_{n=1}^{N} h_{\mu,n}^{illu} P \leq \mathcal{I}_{max},$$

$$\mathcal{I}_{avg}^{-} \leq \frac{1}{K_p} \sum_{\mu=1}^{K_p} \sum_{n=1}^{N} h_{\mu,n}^{illu} P \leq \mathcal{I}_{avg}^{+}, \quad P_{min} \leq P/L \leq P_{max},$$

where $\mathcal{I}_{avg}^{+}$ and $\mathcal{I}_{avg}^{-}$ denote the $\pm 5\%$ of $\mathcal{I}_{avg}$. Furthermore, $h_{\mu,n}^{illu}$ denotes the luminous flux of the unit optical power provided by the nth AP at the μth point of the K_p equally partitioned receiver plane, which is given as

$$h_{\mu,n}^{illu} = \frac{(m_L+1)}{2\pi d^2 \delta} \cos^{m_L}(\theta) \cos(\psi), \tag{13}$$

where δ denotes the optical power to luminous flux conversion factor [14]. Similarly, we also find the maximum optical power $P_{max}^{illu} = \max P$ capable of satisfying the constraints of (12). Note that having predefined illumination requirements also prevents the saturation of the PD receiver, hence we assume the absence of any further clipping at the receiver. As a result, by taking into account both the illumination requirements and LED's physical limits, we have the optical constraint of

$$\max\{P_{min}^{illu}, P_{min}\} \leq P/L \leq \min\{P_{max}^{illu}, P_{max}\}. \tag{14}$$

In this paper, we fix the DC-bias component [5] and assume only negative clipping is incurred by our ACO-OFDM scheme, because we can always set an appropriate margin for preventing upper clipping imposed by the high Peak to Average Power Ratio (PAPR) of ACO-OFDM TD signal samples by controlling the maximum optical output power. More explicitly, to avoid insufficient forward biasing, we set the DC-bias component to be at least as high as the minimum optical power required for satisfying the LED's dynamic range. On the other hand, we also adjust the DC-bias component to 'just' satisfy the predefined illumination requirement. Hence, we have $P^{dc}/L = \max\{P_{min}^{illu}, P_{min}\}$ and the optical requirement of (14) becomes $0 \leq P^{o}/L \leq P_{max}^{o}$, where

$$P_{max}^{o} = \min\{P_{max}^{illu}, P_{max}\} - \max\{P_{min}^{illu}, P_{min}\}, \tag{15}$$

represents the maximum tolerable additional optical power of each LED, so that the communication function would not violate the illumination and LED instrument requirements.

[5]We fix the DC-biasing by focusing our attention on the communications-related energy efficiency maximisation, despite the possibility of adaptive signal scaling and DC biasing [37]. Note that, when DCO-OFDM is considered, optimising the DC-bias component becomes critical [30].

C. System-level Optimisation

Let us now discuss the system-level energy efficiency maximisation. Our forthcoming elaborations are equally applicable both to the conventional cells and to the proposed A-Cells.

1) Formulation: Let us formulate our energy efficiency maximisation problem by defining system's mean energy efficiency on a per-cell basis as

$$\max_{\mathcal{P}} \mathrm{EE} = \frac{1}{|\mathcal{C}|} \sum_{c} \mathrm{EE}_c(\mathcal{P}), \tag{16}$$

We may also define a *global* energy efficiency as the sum throughput of all cells divided by the total power consumption of all cells, where a centralised approach has to be used. By contrast, the *per-cell* basis definition of (16) supports a more scalable and efficient distributed approach. Since $|\mathcal{C}|$ is a constant, (16) can be solved equivalently by optimising $\max_{\mathcal{P}} \sum_c \mathrm{EE}_c(\mathcal{P})$, explicitly

$$\max_{\boldsymbol{P}} \sum_{c\in\mathcal{C}_{vt}} \frac{f_{t,c}^{vt}(\boldsymbol{P})}{f_{p,c}^{vt}(\boldsymbol{P}_c^{vt})} + \sum_{c\in\mathcal{C}_{ct}} \frac{f_{t,c}^{ct}(\boldsymbol{P})}{f_{p,c}^{ct}(\boldsymbol{P}_c^{ct})} \quad \text{s.t.} \quad \mathrm{C1}, \mathrm{C2}, \tag{17}$$

where $\mathcal{C}_{vt}$ and $\mathcal{C}_{ct}$ are the sets hosting the specific cells that employ VT and CT, respectively. Furthermore, we have $\boldsymbol{P} = \{\boldsymbol{P}^{vt}; \boldsymbol{P}^{ct}\}$ acting as the power allocation strategy, which is constituted by that of all VT-aided cells $\boldsymbol{P}^{vt} = \{\boldsymbol{P}_c^{vt}, \forall c \in \mathcal{C}_{vt}\}$ and all CT-aided cells $\boldsymbol{P}^{ct} = \{\boldsymbol{P}_c^{ct}, \forall c \in \mathcal{C}_{vt}\}$, where $\boldsymbol{P}_c^{vt}$ and $\boldsymbol{P}_c^{ct}$ are the power allocation strategy for the cth cell using VT and CT, respectively. By scrutinising (17), we find that only those cells in $\mathcal{C}_{vt}$ and $\mathcal{C}_{ct}$ are included in our optimisation. This implies that those APs, which are not included in $\mathcal{C}_{vt}$ and $\mathcal{C}_{ct}$, are switched into their idle mode.

Still referring to (17), since ACO-OFDM is employed, we can assume Gaussian signalling for $x_k[m]$ in (11) and for $x_{k_0}[m]$ in (9). Hence, we arrive at

$$f_{t,c}^{vt}(\boldsymbol{P}) = \sum_{k\in\mathcal{K}_c} \underbrace{\kappa \log_2 \left[1 + \frac{(\gamma^2/2) P_{c,k}^{vt}}{\sigma^2 + I_{c,k}(\boldsymbol{P}_{\bar{c}}^{vt}, \boldsymbol{P}^{ct})}\right]}_{f_{t,c,k}^{vt}(P_{c,k}^{vt}, \boldsymbol{P}_{\bar{c}}^{vt}, \boldsymbol{P}^{ct})}, \tag{18}$$

$$f_{t,c}^{ct}(\boldsymbol{P}) = \kappa \log_2 \left[1 + \frac{(\gamma^2/2) \left(\sum_{n\in\mathcal{N}_c} h_{k_0,n} \sqrt{P_{c,n}^{ct}}\right)^2}{\sigma^2 + I_{c,k_0}(\boldsymbol{P}_{\bar{c}}^{ct}, \boldsymbol{P}^{vt})}\right], \tag{19}$$

where $\kappa = (1-p)B/4$ is a constant, with the factor of 4 representing the bandwidth efficiency loss owing to the employment of ACO-OFDM having a bandwidth of B and p denoting the blocking probability. Furthermore, $I_{c,k}(\cdot)$ denotes the interference imposed on the kth user in the cth VT-aided cell, while $I_{c,k_0}(\cdot)$ denotes the interference imposed on the only user k_0 in the cth CT-aided cell. In (18) and (19), $\boldsymbol{P}_{\bar{c}}^{vt}$ and $\boldsymbol{P}_{\bar{c}}^{ct}$ represent the power allocation excluding the cth cell

from all VT-aided and CT-aided cells, respectively, which are used for evaluating the interference terms $I_{c,k}(\cdot)$ and $I_{c,k_0}(\cdot)$. Finally, since the DC-bias component is fixed for illumination, we consider the communications-related power consumption in the electronic domain, which may be written as

$$f_{p,c}^{vt}(\boldsymbol{P}_c) = \sum_{n\in\mathcal{N}_c}\sum_{k\in\mathcal{K}_c} g_{n,k}^2 P_{c,k}^{vt}, \tag{20}$$

$$f_{p,c}^{ct}(\boldsymbol{P}_c) = \sum_{n\in\mathcal{N}_c} P_{c,n}^{ct}, \tag{21}$$

where $g_{n,k}$ is the $[n,k]$th entry of the TPC matrix $\boldsymbol{G}$ [6]. Furthermore, as far as the optimisation constraints are concerned, we impose the per-LED optical power constraint pair C1 of

$$\frac{1}{L}\sqrt{\sum_{k\in\mathcal{K}_c} g_{n,k}^2 P_{c,k}^{vt}/2\pi} \le P_{max}^o \qquad \forall n\in\mathcal{N}_c, \forall c\in\mathcal{C}_{vt}, \tag{22}$$

$$\frac{1}{L}\sqrt{P_{c,n}^{ct}/2\pi} \le P_{max}^o \qquad \forall n\in\mathcal{N}_c, \forall c\in\mathcal{C}_{ct}. \tag{23}$$

We also impose the per-user throughput constraint pair C2 for guaranteeing a minimum required QoS as

$$f_{t,c,k}^{vt}(P_{c,k}^{vt}, \boldsymbol{P}_{\tilde{c}}^{vt}, \boldsymbol{P}^{ct}) \ge R \qquad \forall k\in\mathcal{K}_c, \forall c\in\mathcal{C}_{vt}, \tag{24}$$

$$f_{t,c}^{ct}(\boldsymbol{P}) \ge R \qquad \forall c\in\mathcal{C}_{ct}. \tag{25}$$

Note that neglecting the per-user throughput constraint pair C2 by unilaterally maximising the energy efficiency results in an ill-defined problem, since the user QoS target is ignored.

2) Transformation: The objective function defined in (17) is complex due to the coupled nature of the power allocation strategy. Hence, we opt for decoupling the original problem formulated in (17) so as to allow efficient distributed processing. More explicitly, instead of evaluating the true interference term of (18) and (19), we consider the interference upper bound by assuming that all other cells transmit at their maximum permissible optical power. This implies that we carry out *guaranteed* energy efficiency maximisation. More specifically, we use constant $I_{c,k}(P_{max}^o)$ to represent the maximum possible interference imposed on the kth user in the cth VT-aided cell, which is written as

$$I_{c,k}(P_{max}^o) = \gamma^2\pi \sum_{\tilde{c}\in\mathcal{C},\tilde{c}\neq c}\sum_{n\in\mathcal{N}_{\tilde{c}}} h_{k,n}^2 \left(LP_{max}^o\right)^2. \tag{26}$$

Similarly, by replacing $k=k_0$ in (26), we have $I_{c,k_0}(P_{max}^o)$ representing the maximum possible interference imposed on the only user k_0 in the cth CT-aided cell. Correspondingly, we can reformulate the lower bound of (18) and (19) as

$$f_{t,c}^{vt,l}(\boldsymbol{P}_c^{vt}) = f_{t,c}^{vt}(\boldsymbol{P})_{\{I_{c,k}(\boldsymbol{P}_{\tilde{c}}^{vt},\boldsymbol{P}^{ct})\mapsto I_{c,k}(P_{max}^o),\forall k\in\mathcal{K}_c\}}, \tag{27}$$

$$f_{t,c}^{ct,l}(\boldsymbol{P}_c^{ct}) = f_{t,c}^{ct}(\boldsymbol{P})_{\{I_{c,k_0}(\boldsymbol{P}_{\tilde{c}}^{ct},\boldsymbol{P}^{vt})\mapsto I_{c,k_0}(P_{max}^o)\}}. \tag{28}$$

It is plausible that (27) and (28) become only the function of the power allocation strategy of the cth cell, which is decoupled from other cells. Furthermore, since the composition in (19) or in its lower bound expression of (28) results in a non-concave function, we rely on the lower bounding of (28) in order to arrive at the concave formulation of

$$f_{t,c}^{ct,ll}(\boldsymbol{P}_c^{ct}) = \kappa\log_2\left[1+\frac{(\gamma^2/2)\sum_{n\in\mathcal{N}_c} h_{k_0,n}^2 P_{c,n}^{ct}}{\sigma^2 + I_{c,k_0}(P_{max}^o)}\right]. \tag{29}$$

Upon taking into account (27) and (29), we arrive at the new constraint pair C2 formulated as

$$f_{t,c,k}^{vt,l}(P_{c,k}^{vt}) \ge R \qquad \forall k\in\mathcal{K}_c, \forall c\in\mathcal{C}_{vt}, \tag{30}$$

$$f_{t,c}^{ct,ll}(\boldsymbol{P}_c^{ct}) \ge R \qquad \forall c\in\mathcal{C}_{ct}. \tag{31}$$

Clearly, this new constraint pair is more strict than the original constraint pair of (24) and (25). Lastly, the constraint pair C1 remains the same, as in (22) and (23).

Following the above transformation, the decoupled energy efficiency maximisation problem becomes

$$\max_{\boldsymbol{P}} \sum_{c\in\mathcal{C}_{vt}} \frac{f_{t,c}^{vt,l}(\boldsymbol{P}_c^{vt})}{f_{p,c}^{vt}(\boldsymbol{P}_c^{ct})} + \sum_{c\in\mathcal{C}_{ct}} \frac{f_{t,c}^{ct,ll}(\boldsymbol{P}_c^{ct})}{f_{p,c}^{ct}(\boldsymbol{P}_c^{ct})} \tag{32}$$
$$\text{s.t.} \quad (22),(23),(30),(31).$$

Hence, the problem formulated in (32) can be solved in form of $|\mathcal{C}|$ parallel sub-problems, where we have

$$\max_{\boldsymbol{P}_c^{vt}} \frac{f_{t,c}^{vt,l}(\boldsymbol{P}_c^{vt})}{f_{p,c}^{vt}(\boldsymbol{P}_c^{vt})} \qquad \text{s.t.} \quad (22),(30) \quad \forall c\in\mathcal{C}_{vt}, \tag{33}$$

$$\max_{\boldsymbol{P}_c^{ct}} \frac{f_{t,c}^{ct,ll}(\boldsymbol{P}_c^{ct})}{f_{p,c}^{ct}(\boldsymbol{P}_c^{ct})} \qquad \text{s.t.} \quad (23),(31) \quad \forall c\in\mathcal{C}_{ct}. \tag{34}$$

Both (33) and (34) constitute fractional programming problems, which may be solved using Dinkelbach's method [38] by iteratively optimise the subtractive form of (33) and (34). More explicitly, for a particular $c\in\mathcal{C}_{vt}$, the procedures are

1) Introduce the parameter $t_{c,i}^{vt}$ with i being the iteration index and initialise the parameter as $t_{c,1}^{vt}=0$.
2) At each iteration i, solve the inner optimisation problem of the subtractive form of (33), namely

$$\max_{\boldsymbol{P}_c^{vt}} f_{t,c}^{vt,l}(\boldsymbol{P}_c^{vt}) - t_{c,i}^{vt} f_{p,c}^{vt}(\boldsymbol{P}_c^{vt}) \quad \text{s.t.} \quad (22),(30).$$

Since the above inner optimisation problem is a concave maximisation problem, the classic dual-decomposition method yields a zero duality gap and hence achieves optimality. Owing to its popularity in solving convex problems, we refer readers for further details to [39].
3) Let $\boldsymbol{P}_c^{vt,*}$ denote the optimal solutions found for the inner optimisation problem, if we have

$$f_{t,c}^{vt,l}(\boldsymbol{P}_c^{vt,*}) - t_{c,i}^{vt} f_{p,c}^{vt}(\boldsymbol{P}_c^{vt,*}) \le \zeta, \tag{35}$$

then the pre-defined convergence threshold ζ is satisfied, where $\boldsymbol{P}_c^{vt,*}$ constitutes the ultimate solution. Alternatively, if the maximum number of iterations ς is reached, we output $\boldsymbol{P}_c^{vt,*}$ as the ultimate solution. Otherwise, we update the parameters according to

$$t_{c,i+1}^{vt} = f_{t,c}^{vt,l}(\boldsymbol{P}_c^{vt,*}) / f_{p,c}^{vt}(\boldsymbol{P}_c^{vt,*}), \tag{36}$$

and repeat Steps 2 and 3.

[6] We only consider transmission power as our source of power consumption in (20) and (21). In our future work, other sources of power consumption, such as the signal processing costs, back-haul power consumption etc would be desired to paint the whole picture in terms of the entire *network* power consumption [29]. However, at the time of writing, quantifying the network power consumption for VLC systems remains an open issue, since integrating it with a certain VLC back-haul requires dedicated treatment.

The above procedures, referred to as the *baseline algorithm* [7], can be also used for the energy efficiency maximisation of (34) for CT-aided cells and we do not duplicate it here.

3) Simplification: The baseline algorithm requires a number of iterations to converge, where within each iteration, the classic dual-decomposition method invoked, again, requires encapsulated iterations to converge. Hence, we propose an algorithm, which dispenses with the above sophistication.

For any particular VT-aided cell $c \in \mathcal{C}_{vt}$, we use the straightforward equal power allocation strategy of

$$P_{c,k}^{vt} = P_c^{vt} \qquad \forall k \in \mathcal{K}_c. \tag{37}$$

To satisfy the constraint (30), we have

$$P_{c,k}^{vt} \geq (2^{R/\kappa} - 1)[\sigma^2 + I_{c,k}(P_{max}^o)]2/\gamma^2 = P_{c,k}^{vt,l}, \tag{38}$$

$$P_c^{vt} \geq \max_{k \in \mathcal{K}_c} P_{c,k}^{vt,l} = P_c^{vt,l}, \tag{39}$$

while to satisfy the constraint (22), we have

$$P_c^{vt} \leq 2\pi (L P_{max}^o)^2 / \sum_{k \in \mathcal{K}_c} g_{n,k}^2 = P_c^{vt,u}. \tag{40}$$

As a result, provided that $P_c^{vt,l} \leq P_c^{vt,u}$, we have

$$P_c^{vt} = P_c^{vt,l}. \tag{41}$$

The solution P_c^{vt} in (41) ensures that even the least privileged user $k_w = \arg\max_{k \in \mathcal{K}_c}\{I_{c,k}(P_{max}^o)\}$ satisfies the per-user throughput constraint of (30). However, setting P_c^{vt} for other users may 'over-satisfy' their per-user throughput constraint of (30), which leads to an energy efficiency loss. Hence, we improve the above equal power allocation strategy as

1) Let $\mathcal{K}_c^f$ be the set hosting those users with fixed power allocation strategies, which is initialised as $\mathcal{K}_c^f = \{k_w\}$. Let $\mathcal{K}_c^p$ be the complement set of $\mathcal{K}_c^f$ hosting those users with adjustable power allocation strategies. Finally, we initialise $\boldsymbol{A} = \{P_{c,k \in \mathcal{K}_c}^{vt} = P_c^{vt}\}$.
2) For $k \in \mathcal{K}_c^p$, we reduce the power allocated from $P_{c,k}^{vt} = P_c^{vt}$ given in (41) to $P_{c,k}^{vt} = P_{c,k}^{vt,l}$ given in (38). This will result in the adjusted power allocation strategy of

$$\boldsymbol{A}_k = \{P_{c,k}^{vt} = P_{c,k}^{vt,l}, \boldsymbol{\Omega}_k\}, \tag{42}$$

$$\boldsymbol{\Omega}_k = \{P_{c,j \in \mathcal{K}_c^f}^{vt} = P_{c,j}^{vt,l}, P_{c,\tilde{k} \in \mathcal{K}_c^p, \tilde{k} \neq k}^{vt} = P_c^{vt}\}. \tag{43}$$

3) Repeating Step 2 for all users in $\mathcal{K}_c^p$ leads to $|\mathcal{K}_c^p|$ adjusted power allocation strategies $\{\boldsymbol{A}_k, k \in \mathcal{K}_c^p\}$, where we find the one gives the highest energy efficiency

$$k_p = \arg\max_{k \in \mathcal{K}_c^p} \{f_{t,c}^{vt,l}(\boldsymbol{A}_k)/f_{p,c}^{vt}(\boldsymbol{A}_k)\}. \tag{44}$$

4) If we have

$$f_{t,c}^{vt,l}(\boldsymbol{A}_{k_p})/f_{p,c}^{vt}(\boldsymbol{A}_{k_p}) \geq f_{t,c}^{vt,l}(\boldsymbol{A})/f_{p,c}^{vt}(\boldsymbol{A}), \tag{45}$$

then we include k_p in $\mathcal{K}_c^f$ by excluding it from $\mathcal{K}_c^p$ and set $\boldsymbol{A} = \boldsymbol{A}_{k_p}$. Then we repeat the procedure commencing from Step 2. The adjustment stops, when (45) is not met and we output $\boldsymbol{P}_c^{vt,*} = \boldsymbol{A}$.

[7]Other methods solving fractional programming, such as bisection and Charnes-Cooper method, are also interesting but they are beyond our scope.

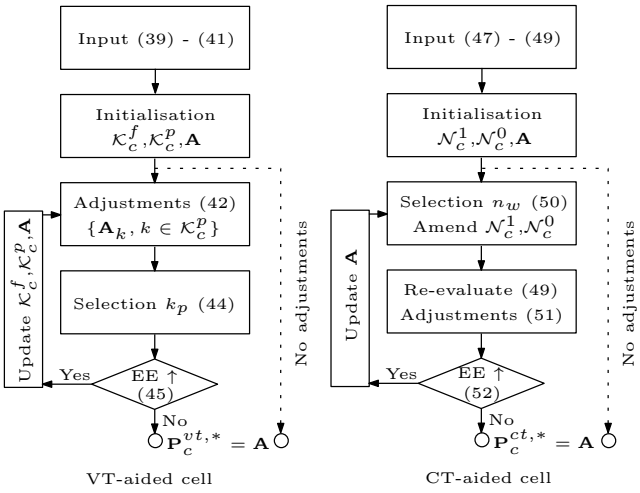

Fig. 2: Flowcharts of the proposed algorithm.

For any particular CT-aided cell $c \in \mathcal{C}_{ct}$, we use the equal power allocation strategy, namely

$$P_{c,n}^{ct} = P_c^{ct} \qquad \forall n \in \mathcal{N}_c. \tag{46}$$

To satisfy the constraint (31), we have

$$P_c^{ct} \geq \frac{(2^{R/\kappa} - 1)[\sigma^2 + I_{c,k_0}(P_{max})]}{(\gamma^2/2)\sum_{n \in \mathcal{N}_c} h_{k_0,n}^2} = P_c^{ct,l}, \tag{47}$$

while to satisfy the constraint (23), we have

$$P_c^{ct} \leq 2\pi (L P_{max}^o)^2 = P_c^{ct,u}. \tag{48}$$

As a result, provided that $P_c^{ct,l} \leq P_c^{ct,u}$, we have

$$P_c^{ct} = P_c^{ct,l}. \tag{49}$$

Let us now adjust the equal power allocation strategy by turning off the communications function for those APs exhibiting high-attenuation channels, since blindly allocating power to it may lead to energy efficiency loss. More explicitly

1) Let $\mathcal{N}_c^0$ and $\mathcal{N}_c^1$ be the set hosting the specific APs whose communication functions are turned off and turned on, respectively, where we have $\mathcal{N}_c^0 = \varnothing$ and $\mathcal{N}_c^1 = \mathcal{N}_c$. Initialise $\boldsymbol{A} = \{P_{c,n \in \mathcal{N}_c}^{ct} = P_c^{ct}\}$.
2) Locate the weakest AP

$$n_w = \arg\min_{n \in \mathcal{N}_c^1} \{h_{k_0,n}\}, \tag{50}$$

and include it in $\mathcal{N}_c^0$ by excluding it from $\mathcal{N}_c^1$.
3) Re-evaluate (47) and (48) using $\mathcal{N}_c^1$ instead of $\mathcal{N}_c$ in order to get $P_c^{ct,1}$. Hence, we arrive at the new power allocation strategy of

$$\boldsymbol{A}_{n_w} = \{P_{c,n \in \mathcal{N}_c^0}^{ct} = 0, P_{c,n \in \mathcal{N}_c^1}^{ct} = P_c^{ct,1}\}. \tag{51}$$

4) If we have

$$f_{t,c}^{ct,ll}(\boldsymbol{A}_{n_w})/f_{p,c}^{ct}(\boldsymbol{A}_{n_w}) \geq f_{t,c}^{ct,ll}(\boldsymbol{A})/f_{p,c}^{ct}(\boldsymbol{A}), \tag{52}$$

we set $\boldsymbol{A} = \boldsymbol{A}_{n_w}$ and repeat the above procedure, commencing from Step 2. The adjustments stop when (52) is not met and we output $\boldsymbol{P}_c^{ct,*} = \boldsymbol{A}$.

TABLE I: List of Parameters

LED-related Parameters	
semi-angle at half-illumination $\phi_{1/2}$	60^o
gain of optical filter $f_{of}(\psi)$	1
physical area for a PD receiver A_{PD}	1 cm^2
O/E conversion factor γ	0.53 A/W
refractive index n_r	1.5
half of the receiver's FoV ψ_F	45^o
Vishay TSHG8200 LED min optical power P_{min}	5 mW
Vishay TSHG8200 LED max optical power P_{max}	50 mW
optical power to luminous flux conversion factor δ	2.1 mW/lm
Environment-related Parameters	
room size	15×15×3 m^3
user height	0.85 m
number of users (change in Fig 5)	20 (uniform)
AP height	2.5 m
number of APs	8×8 (uniform)
LED array per AP	15×15
reflection efficiency ρ	0.75
illumination requirement $[\mathcal{I}_{min}, \mathcal{I}_{max}, \mathcal{I}_{avg}]$	[200,800,600]
modulation bandwidth B	20 MHz
blocking probability p (change in Fig 4)	0
Baseline Algorithm-related Parameters	
maximum iterations ς (change in Fig 6)	20
convergence threshold ζ	0.01

Remark II-C3: If no power adjustments are carried out, the algorithm proposed for the VT-aided or CT-aided cells only requires a one-off evaluation of (41) or (49), respectively. When adjustments are indeed required, the algorithm proposed requires at most $|\mathcal{K}_c|-1$ or $|\mathcal{N}_c|-1$ additional iterations for the VT-aided or CT-aided cells, respectively. Within each iteration, the dominant complexity component is only linearly increasing according to the order of $\mathcal{O}(\mathcal{K}_c^p)$ or $\mathcal{O}(\mathcal{N}_c^1)$ associated with evaluating (44) or (50) for the VT-aided or CT-aided cells, respectively. To further aid the reader's understanding, a flow chart is included in Fig 2.

III. Numerical Results

Let us now provide simulation results for characterising the energy efficiency of the indoor VLC system relying on the amorphous structure. All our simulations are carried out for 100 random independent snapshots of the user distributions using the parameters included in Table I.

A. Comparisons

For fair comparisons, in Fig 3, the same transmission strategy is employed and the same baseline optimisation algorithm is applied for all the cell formation strategies involved, where we have set the minimum per-user throughput constraint to $R = 15$ MBits/s for our optimisation algorithm.

1) Edge-Distance based A-Cells v.s. Conventional Cells: The left subplot of Fig 3 compares the energy efficiency per user between the conventional cells and the edge-distance based A-Cells having 20 users (hollow) and 25 users (solid). Explicitly, 'E3.5' stands for the edge-distance based A-Cells having $d_0 = 3.5$m. This value of d_0 was specifically selected to result in an average number of cells, which is similar to that of the bench-marker scenario 'S16'. We also included the bench-marker scenario 'S1' as introduced in Section II-A2. Since similar trends may also be found for the centroid-distance based A-Cells, we omit them for space economy.

It can be seen from the left subplot of Fig 3 that, for both 20 users and 25 users, the edge-distance based A-Cells exhibit a consistently higher energy efficiency per user than both the conventional cell formations 'S16' and 'S1', where the relative energy efficiency becomes significantly greater upon increasing the FoVs when experiencing more interference. Quantitatively, when having 20 users, the edge-distance based A-Cells are capable of achieving over 4 times (nearly 10 times) energy efficiency per user than that of the bench-marker scenario 'S1' at FoV of 95^o (of 100^o). Similarly, when compared to the bench-marker scenario 'S16', the edge-distance based A-Cells are capable of roughly doubling the energy efficiency per user at both FoVs of 95^o and of 100^o. These observations imply that the advocated edge-distance based A-Cells are capable of handling scenarios having more interference. This is true upon slightly increasing the number of users from 20 to 25, where the edge-distance based A-Cells achieve overwhelmingly higher energy efficiency per user than both conventional cell formations 'S16' and 'S1'.

Furthermore, we included the classic scheme of frequency reuse having a factor of two in conjunction with both the conventional cell formations 'S16' and 'S1'. It can be seen from the left subplot of Fig 3 that the edge-distance based A-Cells exhibit a consistently higher energy efficiency per user than both the conventional cell formations relying on frequency reuse for all FoV settings and for both user settings. For all FoVs, as expected, the higher the number of users, the higher the energy efficiency per user of the edge-distance based A-Cells becomes in comparison to both conventional cell formations. Upon increasing the FoVs, the energy efficiency per user achieved by the edge-distance based A-Cells is reduced for both conventional cell formations as well as for both user settings, exhibiting a steeper reduction for the conventional cell formation 'S1'. This is because, the higher the FoV, the more interference is encountered, hence frequency reuse becomes more beneficial. Despite this reduction, the energy efficiency per user achieved by the edge-distance based A-Cells remains at least three times higher when compared to that of the conventional cell formation 'S1' employing frequency reuse and supporting 20 users. To sum up, the edge-distance based A-Cells are significantly more energy efficient than both the conventional cell formations 'S16' and 'S1' operating with or without frequency reuse.

2) Edge-Distance v.s. Centroid-Distance based A-Cells: Owing to the flexibility of the distance based A-Cells, we can appropriately configure them to provide a fair comparison. The right subplot of Fig 3 compares the energy efficiency per user between the edge-distance (hollow) and the centroid-distance (solid) based A-Cells with the average number of A-Cells spanning from 1 to 6. For the edge-distance based A-Cells, we evaluate $d_0 = [3, 3.5, 4, 4.5, 5]$, while for the centroid-distance based A-Cells, we evaluate $d_0 = [5, 6, 7, 8, 9]$. Note that the higher the value of d_0, the smaller the average number of resultant A-Cells. It can be seen from the right subplot of Fig 3 that the edge-distance based A-Cells exhibit a consistently higher energy efficiency per user than that of the centroid-distance based A-Cells for all resultant average number of A-Cells and for all FoVs, which shows the superiority of

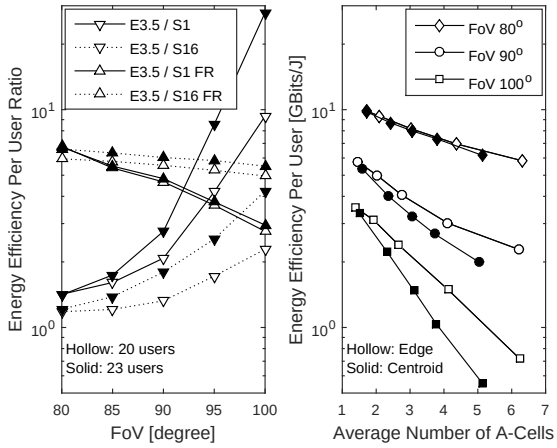

Fig. 3: Energy efficiency per user comparisons of various cell formation strategies (left) as well as between the edge and centroid-distance based A-Cells (right) using the parameters of Table I.

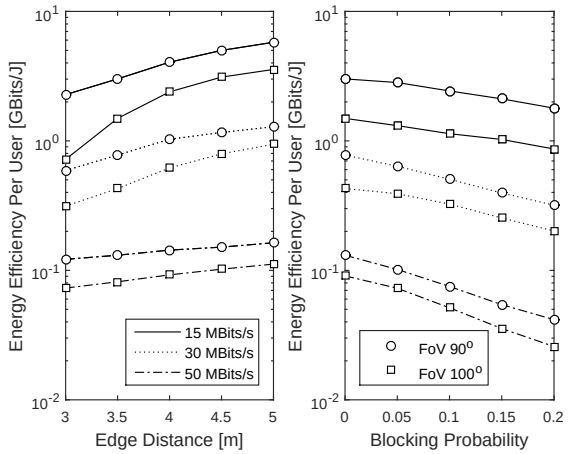

Fig. 4: Energy efficiency per user for edge-distance based A-Cells as a function of the predefined edge-distance threshold (left) and of the LoS and reflected-path blocking probability (right) using the parameters of Table I.

the edge-distance based A-Cells. Indeed, we observe that the superiority of the edge-distance based A-Cells is more prominent at higher FoVs for all resultant average number of A-Cells, while they become very similar at FoV of 80^o. Finally, at FoVs of 90^o and of 100^o, we observe that the superiority of edge-distance based A-Cells is greater when having a larger number of resultant A-Cells, whilst there are marginal differences when the number of A-Cells is small.

B. Details

We now provide detailed observations regarding the edge-distance based A-Cells. In these investigations, we use our baseline algorithm for optimisation. Since similar trends may also be found for the centroid-distance based A-Cells, we omit them for space economy.

1) Effect of Edge Distance: The left subplot of Fig 4 shows the energy efficiency per user for edge-distance based A-Cells as a function of the predefined edge-distance threshold. It can be seen from the left subplot of Fig 4 that as expected, guaranteeing a higher per-user throughput incurs an energy efficiency loss compared to requiring a lower per-user throughput for all predefined edge-distance threshold settings and for both FoVs, demonstrating that any throughput improvement requires extra power to be invested [8]. Furthermore, for all throughput constraints and for all predefined edge-distance threshold settings, having a higher FoV results in a consistently lower energy efficiency per user than that of a lower FoV, since more interference is encountered and more APs are involved when having a higher FoV. Finally, we observe that the higher the edge-distance threshold, the higher the energy efficiency per user becomes for all throughput constraints and for both FoVs. However, at this stage, we are reluctant to claim the superiority of setting towards higher edge-distance threshold for the reasons discussed as follows.

In principle, setting a lower edge-distance threshold results into several decoupled A-Cells, whilst having a higher edge-distance threshold results into a few large A-Cells. In both settings, the total number of participated APs remains similar under a given FoV. Having a few large A-Cells creates a large-dimensional multi-user MISO system. Hence, it is capable of more easily satisfying a given throughput constraint than forming several decoupled A-Cells. However, having a large-dimensional multi-user MISO system will potentially incur additional signal processing costs, such as the inversion of a large matrix at the distributed APs as required by the ZF based TPC. Also, sharing data amongst APs of large A-Cells may require more capable back-haul. Hence, network power consumption by additionally considering the signal processing costs and back-haul power consumption is required to determine the most appropriate edge-distance threshold.

2) Effect of Blocking: The right subplot of Fig 4 shows the energy efficiency per user for edge-distance based A-Cells associated with $d_0 = 3.5$m as a function of the LoS and reflected-path blocking probability. It can be seen from the right subplot of Fig 4 that as expected, the higher the blocking probability, the lower the energy efficiency per user becomes for all throughput constraints and for both FoVs. Furthermore, for all blocking probabilities and for both FoVs, the energy efficiency per user is higher for a lower throughput constraint than for a higher throughput constraint. We observe also that, the slope of the energy efficiency reduction per user is higher for a higher throughput constraint for both FoVs. Finally, for all throughput constraints and for all blocking probabilities, having a higher FoV results in a consistently lower energy efficiency per user than that of a lower FoV, since more interference is encountered and more APs are involved when having a higher FoV. Note that, the blocking model considered here is independent of the FoVs, while we will consider a more realistic FoV-related blocking in the future.

[8]Different modulations incur different levels of energy investments. For example, Color Shift Keying (CSK) relies on the LEDs' color mapping capability, instead of higher DC power, for achieving an increased data rate.

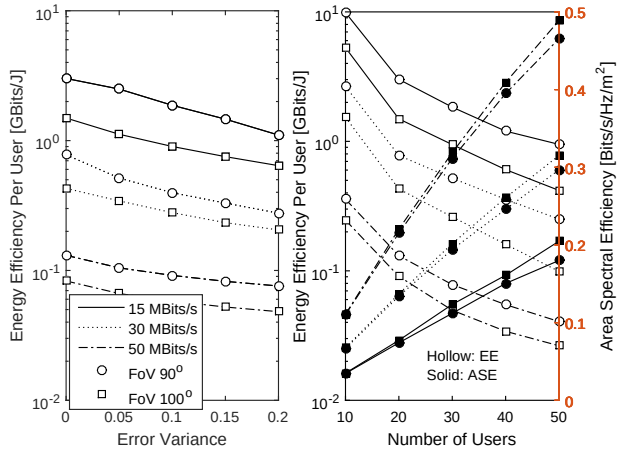

Fig. 5: Energy efficiency per user for edge-distance based A-Cells associated with $d_0 = 3.5$m as a function of error variance (left) and energy efficiency per user versus area spectral efficiency trade-offs (right) as a function of user density using the parameters of Table I.

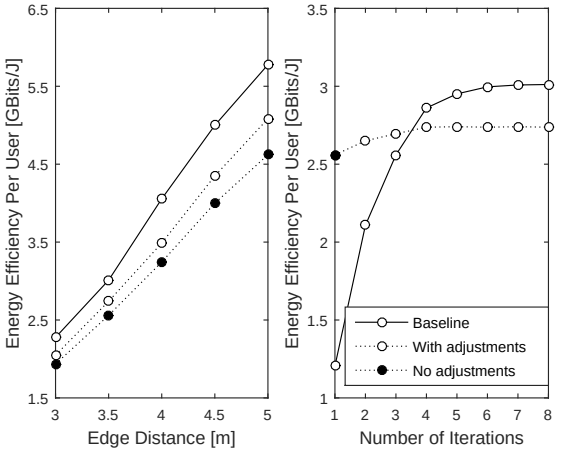

Fig. 6: Energy efficiency per user for edge-distance based A-Cells as a function of the predefined edge-distance threshold (left) and of the number of iterations (right) when using both the baseline algorithm and the proposed algorithm with and without adjustments and using the parameters of Table I.

3) Effect of Imperfect Channel Knowledge: The left of Fig 5 shows the energy efficiency per user for edge-distance based A-Cells associated with $d_0 = 3.5$m as a function of the error variance of imperfect channel knowledge at the distributed APs used for VT or CT. We assumed Gaussian distributed errors and as expected, the achievable energy efficiency per user degrades upon increasing the error variance for all throughput constraints and for both FoVs. Furthermore, for all error variances and for both FoVs, the energy efficiency per user is higher for a lower throughput constraint than for a higher throughput constraint. Furthermore, for all throughput constraints and for all error variances, having a higher FoV results in a consistently lower energy efficiency per user than that of a lower FoV. These investigations imply the importance of having an accurate channel knowledge, where a modest reduction may be observed in the left of Fig 5 at an error variance of 0.2 for all throughput constraints and for both FoVs. Hence, a classic trade-off arises between reducing the error variance and investing extra cost, which will be set aside for our future work.

4) Effect of User Density: The right subplot of Fig 5 shows the energy efficiency per user for edge-distance based A-Cells associated with $d_0 = 3.5$m as a function of user density. It can be seen from the right subplot of Fig 5 that as expected for all throughput constraints and for both FoVs, the higher the number of users, the lower the energy efficiency per user becomes, since the interference becomes more pervasive and more number of APs are involved. Importantly, the most substantial drop appears upon increasing the number of users from 10 to 20, followed by a less dramatic energy efficiency erosion per user beyond 20 users. Furthermore, for all user density settings and for both FoVs, the energy efficiency per user is higher for a lower throughput constraint than for a higher throughput constraint. Finally, for all throughput constraints and for all user density settings, having a higher FoV results in a consistently lower energy efficiency per user than that of a lower FoV, since more interference is encountered and more APs are involved when having a higher FoV.

5) Trade-offs: The right subplot of Fig 5 also shows the Area Spectral Efficiency (ASE) for edge-distance based A-Cells associated with $d_0 = 3.5$m as a function of user density. It can be seen from the right subplot of Fig 5 that as expected, for all user density settings and for both FoVs, the ASE is higher for a higher throughput constraint than for a lower throughput constraint. Furthermore, for all throughput constraints and for both FoVs, the higher the number of users, the higher the ASE becomes. This is because the aggregated throughput is higher for a higher number of users. However, the ASE improvement seen in the right subplot of Fig 5 is achieved at the cost of sacrificing the energy efficiency per user. Achieving a higher ASE at the cost of reducing the energy efficiency contradicts to our original design objective. Similarly, for all throughput constraints and for all user density settings, having a higher FoV results in a slightly higher energy efficiency per user than that of a lower FoV, again at the cost of sacrificing the energy efficiency. Finally, we note that the ASE recorded in the right subplot of Fig 5 is *not* the maximum achievable ASE, since it was evaluated under the specific constraint of the power allocation strategy obtained when using the energy efficiency as our design objective.

C. Algorithms

We now discuss the performance of our proposed algorithm, where we set the minimum per-user throughput constraint to $R = 15$ MBits/s and FoV of 90^o for our investigations.

1) Comparison: The left subplot of Fig 6 shows the energy efficiency per user for edge-distance based A-Cells as a function of the predefined edge-distance threshold, when using both the baseline algorithm and the proposed algorithm with and without adjustments, as detailed in Section II-C3.

For our proposed algorithm relying on adjustments, we set $|\mathcal{K}_c| - 1$ and $|\mathcal{N}_c| - 1$ as the maximum number of iterations for our VT and CT-aided A-Cells, respectively. It can be seen from the left subplot of Fig 6 that the proposed algorithm operating without adjustments is capable of achieving much of the energy efficiency per user obtained by the baseline algorithm. When relying on additional adjustments, the proposed algorithm achieves a higher energy efficiency per user than that of its non-adjusted counterparts. In particular, it performs quite similarly to the baseline algorithm, when the predefined edge-distance threshold is small.

2) Convergence: The right subplot of Fig 6 shows the convergence of both the baseline and of the proposed algorithm for edge-distance based A-Cells associated with $d_0 = 3.5$m. It can be seen that the baseline algorithm converges within 6 iterations with further embedded iterations owing to the usage of the dual-decomposition method. For our proposed algorithm, 3 iterations are typically sufficient to approach convergence dispensing with the dual-decomposition method. Despite the *ultimate* sub-optimality, the *intermediate* energy efficiency per user achieved by our proposed algorithm is much higher than that of the baseline algorithm. This becomes especially prominent, when we only use a single iteration, which is marked by the solid circle. In the right subplot of Fig 6, quantitatively, the achievable energy efficiency per user of our proposed algorithm after 3 iterations accounts for slightly more than 90% that of its ultimate counterpart constituted by our baseline algorithm.

IV. Conclusions

In this paper, we discussed the hitherto-unexplored amorphous structure for constructing energy efficient VLC systems. This problem was approached by the joint design of three inter-linked aspects under the critical consideration of optical constraints. Our numerical results demonstrated that the amorphous structure proposed is beneficial in VLC system design, since it results in a higher energy efficiency than that of the conventional structure. Furthermore, our proposed algorithm is capable of performing close to the baseline algorithm, making it an attractive design alternative. Finally, our proposed amorphous structure constitutes a promising LiFi solution, providing services in various indoor applications, including museums, offices and hospitals. These observations stimulate a range of further research topics, such as the energy efficient VLC system design taking into account the clipping-distortion of DCO-OFDM, the co-design of energy efficient communication and illumination, the network power consumption of VLC system, the comparison to other OOFDM schemes [37], [40], [41], the investigation of non-linear VT, and finally the robust design under channel estimation uncertainties, etc.

References

[1] G. Li, Z. Xu, C. Xiong, C. Yang, S. Zhang, Y. Chen, and S. Xu, "Energy-efficient wireless communications: tutorial, survey, and open issues," *IEEE Wireless Communications*, vol. 18, no. 6, pp. 28–35, Dec 2011.

[2] G. Miao, N. Himayat, and G. Li, "Energy-efficient link adaptation in frequency-selective channels," *IEEE Transactions on Communications*, vol. 58, no. 2, pp. 545–554, Feb 2010.

[3] D. Ng, E. Lo, and R. Schober, "Energy-efficient resource allocation in OFDMA systems with large numbers of base station antennas," *IEEE Transactions on Wireless Communications*, vol. 11, no. 9, pp. 3292–3304, Sep 2012.

[4] S. He, Y. Huang, L. Yang, and B. Ottersten, "Coordinated multicell multiuser precoding for maximizing weighted sum energy efficiency," *IEEE Transactions on Signal Processing*, vol. 62, no. 3, pp. 741–751, Feb 2014.

[5] C. He, B. Sheng, P. Zhu, X. You, and G. Li, "Energy- and spectral-efficiency tradeoff for distributed antenna systems with proportional fairness," *IEEE Journal on Selected Areas in Communications*, vol. 31, no. 5, pp. 894–902, May 2013.

[6] L. B. Le, D. Niyato, E. Hossain, D. I. Kim, and D. T. Hoang, "QoS-aware and energy-efficient resource management in OFDMA femtocells," *IEEE Transactions on Wireless Communications*, vol. 12, no. 1, pp. 180–194, Jan 2013.

[7] S. Rangan, T. Rappaport, and E. Erkip, "Millimeter-wave cellular wireless networks: potentials and challenges," *Proceedings of the IEEE*, vol. 102, no. 3, pp. 366–385, Mar 2014.

[8] L. Hanzo, H. Haas, S. Imre, D. O'Brien, M. Rupp, and L. Gyongyosi, "Wireless myths, realities, and futures: From 3G/4G to optical and quantum wireless," *Proceedings of the IEEE*, vol. 100, no. Special Centennial Issue, pp. 1853–1888, May 2012.

[9] E. Bjornson, L. Sanguinetti, J. Hoydis, and M. Debbah, "Optimal design of energy-efficient multi-user MIMO systems: Is massive MIMO the answer?" *IEEE Transactions on Wireless Communications*, vol. 14, no. 6, pp. 3059–3075, Jun 2015.

[10] R. Zhang, L.-L. Yang, and L. Hanzo, "Energy pattern aided simultaneous wireless information and power transfer," *IEEE Journal on Selected Areas in Communications*, vol. 33, no. 8, pp. 1492–1504, Aug 2015.

[11] R. Zhang, R. Maunder, and L. Hanzo, "Wireless information and power transfer: from scientific hypothesis to engineering practice," *IEEE Communications Magazine (accepted)*, 2015. [Online]. Available: http://eprints.soton.ac.uk/368187/

[12] R. Zhang, J. Wang, Z. Wang, Z. Xu, C. Zhao, and L. Hanzo, "Visible light communications in heterogeneous networks: pave the way for user-centric design," *IEEE Wireless Communications*, vol. 22, no. 2, pp. 8–16, Apr 2015.

[13] T. Komine and M. Nakagawa, "Fundamental analysis for visible-light communication system using LED lights," *IEEE Transactions on Consumer Electronics*, vol. 50, no. 1, pp. 100–107, Feb 2004.

[14] J. Grubor, S. Randel, K.-D. Langer, and J. Walewski, "Broadband information broadcasting using LED-based interior lighting," *Journal of Lightwave Technology*, vol. 26, no. 24, pp. 3883–3892, Dec 2008.

[15] R. Zhang and L. Hanzo, "Multi-layer modulation for intensity-modulated direct-detection optical OFDM," *Journal of Optical Communications and Networking*, vol. 5, no. 12, pp. 1402–1412, Dec 2013.

[16] J. Armstrong, "OFDM for optical communications," *Journal of Lightwave Technology*, vol. 27, no. 3, pp. 189–204, Feb 2009.

[17] A. Azhar, T. Tran, and D. O'Brien, "A Gigabit/s indoor wireless transmission using MIMO-OFDM visible-light communications," *IEEE Photonics Technology Letters*, vol. 25, no. 2, pp. 171–174, Jan 2013.

[18] D. Tsonev, H. Chun, S. Rajbhandari, J. McKendry, S. Videv, E. Gu, M. Haji, S. Watson, A. Kelly, G. Faulkner, M. Dawson, H. Haas, and D. O'Brien, "A 3-Gb/s single-LED OFDM-based wireless VLC link using a gallium nitride μ LED," *IEEE Photonics Technology Letters*, vol. 26, no. 7, pp. 637–640, Apr 2014.

[19] H. Burchardt, N. Serafimovski, D. Tsonev, S. Videv, and H. Haas, "VLC: beyond point-to-point communication," *IEEE Communications Magazine*, vol. 52, no. 7, pp. 98–105, July 2014.

[20] B. Ghimire and H. Haas, "Self-organising interference coordination in optical wireless networks," *EURASIP Journal on Wireless Communications and Networking*, vol. 2012, no. 1, 2012.

[21] D. Bykhovsky and S. Arnon, "Multiple access resource allocation in visible light communication systems," *Journal of Lightwave Technology*, vol. 32, no. 8, pp. 1594–1600, Apr 2014.

[22] M. Biagi, S. Pergoloni, and A. M. Vegni, "LAST: a framework to localize, access, schedule, and transmit in indoor VLC systems," *Journal of Lightwave Technology*, vol. 33, no. 9, pp. 1872–1887, May 2015.

[23] F. Jin, R. Zhang, and L. Hanzo, "Resource allocation under delay-guarantee constraints for heterogeneous visible-light and RF femtocell," *IEEE Transactions on Wireless Communications*, vol. 14, no. 2, pp. 1020–1034, Feb 2015.

[24] X. Li, R. Zhang, and L. Hanzo, "Cooperative load balancing in hybrid visible light communications and WiFi," *IEEE Transactions on Communications*, vol. 63, no. 4, pp. 1319–1329, Apr 2015.

[25] K. Lee and H. Park, "Modulations for visible light communications with dimming control," *IEEE Photonics Technology Letters*, vol. 23, no. 16, pp. 1136–1138, Aug 2011.
[26] I. Din and H. Kim, "Energy-efficient brightness control and data transmission for visible light communication," *IEEE Photonics Technology Letters*, vol. 26, no. 8, pp. 781–784, Apr 2014.
[27] S. Kim and S.-Y. Jung, "Modified Reed Muller coding scheme made from the bent function for dimmable visible light communications," *IEEE Photonics Technology Letters*, vol. 25, no. 1, pp. 11–13, Jan 2013.
[28] Y. Suh, C.-H. Ahn, and J. K. Kwon, "Dual-codeword allocation scheme for dimmable visible light communications," *IEEE Photonics Technology Letters*, vol. 25, no. 13, pp. 1274–1277, July 2013.
[29] R. Razavi and H. Claussen, "Urban small cell deployments: Impact on the network energy consumption," in *IEEE Wireless Communications and Networking Conference Workshops*, Apr 2012, pp. 47–52.
[30] S. Dimitrov, S. Sinanovic, and H. Haas, "Clipping noise in OFDM-based optical wireless communication systems," *IEEE Transactions on Communications*, vol. 60, no. 4, pp. 1072–1081, Apr 2012.
[31] A. Farid and S. Hranilovic, "Capacity bounds for wireless optical intensity channels with gaussian noise," *IEEE Transactions on Information Theory*, vol. 56, no. 12, pp. 6066–6077, Dec 2010.
[32] X. Li, R. Mardling, and J. Armstrong, "Channel capacity of IM/DD optical communication systems and of ACO-OFDM," in *IEEE International Conference on Communications*, Jun 2007, pp. 2128–2133.
[33] S. Dimitrov and H. Haas, "Information rate of OFDM-based optical wireless communication systems with nonlinear distortion," *Journal of Lightwave Technology*, vol. 31, no. 6, pp. 918–929, Mar 2013.
[34] M. Costa, "Writing on dirty paper," *IEEE Transactions on Information Theory*, vol. 29, no. 3, pp. 439–441, May 1983.
[35] J. Lee and N. Jindal, "High SNR analysis for MIMO broadcast channels: Dirty paper coding versus linear precoding," *IEEE Transactions on Information Theory*, vol. 53, no. 12, pp. 4787–4792, Dec 2007.
[36] R. Zhang and L. Hanzo, "Cooperative downlink multicell preprocessing relying on reduced-rate back-haul data exchange," *IEEE Transactions on Vehicular Technology*, vol. 60, no. 2, pp. 539–545, Feb 2011.
[37] Z. Wang, Q. Wang, S. Chen, and L. Hanzo, "An adaptive scaling and biasing scheme for OFDM-based visible light communication systems," *Optics Express*, vol. 22, no. 10, pp. 12 707–12 715, May 2014.
[38] W. Dinkelbach, "On nonlinear fractional programming," *Management Science*, vol. 13, pp. 492–498, Mar 1967.
[39] S. Boyd and L. Vandenberghe, *Convex Optimization*. New York, NY, USA: Cambridge University Press, 2004.
[40] L. Chen, B. Krongold, and J. Evans, "Successive decoding of anti-periodic OFDM signals in IM/DD optical channel," in *IEEE International Conference on Communications*, May 2010, pp. 1–6.
[41] Q. Gao, C. Gong, S. Li, and Z. Xu, "DC-informative modulation for visible light communications under lighting constraints," *IEEE Wireless Communications*, vol. 22, no. 2, pp. 54–60, Apr 2015.

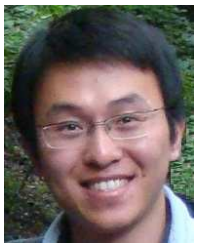

Rong Zhang (M'09) is an assistant professor in Southampton Wireless group within the school of ECS at University of Southampton (UoS). He received his PhD in wireless communications from UoS in 2009, where he was a research assistant during that period with Mobile Virtual Centre of Excellence, one of UK's largest industrial-academic partnership in ICT. During his post-doctoral period in ECS, he contributed as the UoS lead researcher on a number of international projects. After that, he took his industrial consulting leave for Huawei EU R&D as a System Algorithms Expert. He is also a guest researcher of the Centre in Next Generation Computational Modelling at UoS. He has a total of 70+ IEEE/OSA publications, including 40+ journals (20+ of which as first author). Owing to his outstanding academic achievements, he is the recipient of the prestigious Dean's Publication Award. He regularly serves as reviewer for IEEE/OSA journals and has been several times as TPC member/invited session chair of major conferences. He is a member of the IET, of the IEEE and is the recipient of joint funding of MVCE and EPSRC as well as the recipient of Worldwide University Network grant.

Holger Claussen is leader of Small Cells Research at Bell Labs, Alcatel-Lucent. In this role, he and his team are innovating in all areas related to future evolution, deployment, and operation of small cell networks to enable exponential growth in mobile data traffic. His research in this domain has been commercialized in Alcatel-Lucents Small Cell product portfolio and continues to have significant impact. He received the 2014 World Technology Award in the individual category Communications Technologies for innovative work of the greatest likely long-term significance. Prior to this, Holger was head of the Autonomous Networks and Systems Research Department at Bell Labs Ireland, where he directed research in the area of self-managing networks to enable the first large scale femtocell deployments from 2009 onwards. Holger joined Bell Labs in 2004, where he began his research in the areas of network optimization, cellular architectures, and improving energy efficiency of networks. Holger received his Ph.D. degree in signal processing for digital communications from the University of Edinburgh, United Kingdom in 2004. He is author of more than 90 publications and 110 filed patent applications. He is Fellow of the World Technology Network, senior member of the IEEE, and member of the IET.

Harald Haas holds the Chair for Mobile Communications at the School of Engineering, and is the Director of the Li-Fi Research and Development Centre. Professor Haas has been working in wireless communications for 20 years and held several posts in industry. He was an invited speaker at TED Global in 2011 where he demonstrated and coined LiFi. Li-Fi was listed among the 50 best inventions in TIME Magazine 2011. Moreover, his work has been covered in other international media such as the New York Times, BBC, MSNBC, CNN International, Wired UK, and many more. He is initiator, co-founder and chief scientific officer (CSO) of pureLiFi Ltd. Professor Haas holds 31 patents and has more than 30 pending patent applications. He has published 300 conference and journal papers including a paper in Science Magazine. He published two textbooks with Cambridge University Press. His h-index is 43 (Google). In 2015 he was co-recipient of three best paper awards including the IEEE Jack Neubauer Memorial Award. He is CI of programme grant TOUCAN (EP/L020009/1), and CI of SERAN (EP/L026147/1). He currently holds an EPSRC Established Career Fellowship (EP/K008757/1). In 2014, Professor Haas was selected as one of ten EPSRC RISE Campaign Leaders.

Lajos Hanzo FREng, FIEEE, FIET, Fellow of EURASIP, DSc received his degree in electronics in 1976 and his doctorate in 1983. In 2009 he was awarded the honorary doctorate "Doctor Honoris Causa" by the Technical University of Budapest. During his 38-year career in telecommunications he has held various research and academic posts in Hungary, Germany and the UK. Since 1986 he has been with the School of Electronics and Computer Science, University of Southampton, UK, where he holds the chair in telecommunications. He has successfully supervised 80+ PhD students, co authored 20 John Wiley/IEEE Press books on mobile radio communications totalling in excess of 10 000 pages, published 1400+ research entries at IEEE Xplore, acted both as TPC and General Chair of IEEE conferences, presented keynote lectures and has been awarded a number of distinctions. Currently he is directing a 100-strong academic research team, working on a range of research projects in the field of wireless multimedia communications sponsored by industry, the Engineering and Physical Sciences Research Council (EPSRC) UK, the European Research Council's Advanced Fellow Grant and the Royal Society's Wolfson Research Merit Award. He is an enthusiastic supporter of industrial and academic liaison and he offers a range of industrial courses. He is also a Governor of the IEEE VTS. During 2008 - 2012 he was the Editor-in-Chief of the IEEE Press and a Chaired Professor also at Tsinghua University, Beijing. His research is funded by the European Research Council's Senior Research Fellow Grant. For further information on research in progress and associated publications please refer to http://www-mobile.ecs.soton.ac.uk Lajos has 20 000+ citations.